



## Original article

The efficacy of <sup>18</sup>F-FDG PET/CT-based diagnostic model in the diagnosis of colorectal cancer regional lymph node metastasisZhiguang Yang<sup>a</sup>, Zhaoyu Liu<sup>b,\*</sup><sup>a</sup> Nuclear Medicine Department, Shengjing Hospital Affiliated to China Medical University, Shenyang 110000, China<sup>b</sup> Radiology Department, Shengjing Hospital Affiliated to China Medical University, Shenyang 110000, China

## ARTICLE INFO

## Article history:

Received 28 September 2019

Revised 16 November 2019

Accepted 9 December 2019

Available online 19 December 2019

## Keywords:

<sup>18</sup>F-FDG PET/CT

Diagnostic model

Colorectal cancer

Regional lymph node metastasis

## ABSTRACT

In order to assess the efficacy of <sup>18</sup>F-FDG PET/CT-based diagnostic model in diagnosing colorectal cancer (CRC) lymph node metastasis (LNM), the <sup>18</sup>F-FDG PET/CT medical records of CRC patients were acquired, and the CRC regional LNM diagnostic model was constructed through the combination of image and grain factors of <sup>18</sup>F-FDG PET/CT. The specific analysis methods include univariate analysis, multivariate analysis, ROC curve analysis, and statistical analysis. The research results showed statistical differences in TNM staging, intestinal obstructions, tumor infiltration, regional lymph node (LN) SUVmax, regional LN minimum dimension, and remote metastasis between the CRC patients in the LNM positive group and the LNM negative group. Through the comparisons between the diagnostic model proposed in the research and other diagnostic methods, it was found that the AUC (95%CI) and sensitivity of the proposed diagnostic model were the highest, the comprehensive diagnostic efficacy of the diagnostic model was optimal. Therefore, it was concluded that the diagnostic model was of significant application values, which provided the basis for subsequent clinical diagnosis of CRC.

© 2019 The Author(s). Published by Elsevier B.V. on behalf of King Saud University. This is an open access article under the CC BY-NC-ND license (<http://creativecommons.org/licenses/by-nc-nd/4.0/>).

## 1. Introduction

Colorectal cancer (CRC), also known as the tumor of large intestine, is the malignant tumor that occurs in the mucosal epithelium of large intestines (Long et al., 2017). Over the years, the morbidity rate of CRC has increased in most countries worldwide. The morbidity rate of CRC in China is lower than that in European and American countries, which ranks the third place in terms of morbidity rates of malignant tumors and the fifth place of the most fatal malignant tumors in China (Arnold et al., 2017; Rex et al., 2017; Flemer et al., 2017). Most of the patients with CRC are middle-ages and elderly. More than 90% of the patients are at least 50 years old; however, with the changes in lifestyle and diet, the incidence age of CRC is gradually declining (Muro, 2017). The mor-

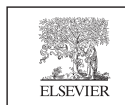
tality of CRC has also increased in recent years. The cause of CRC-related death is mainly tumor recurrence and metastasis. Lymph node metastasis (LNM) is a common and foremost metastasis of CRC, which is also the root reason of tumor recurrence (Yu et al., 2017). The existence or non-existence of regional LNM in patients with CRC is closely related to the tumor TNM staging, the choice of therapeutic plans, and the prognosis. In the selection of therapeutic plans, CRC patient in stage 3 and CRC patients in stage 2 with high-risk factors can make profit from auxiliary chemotherapy; therefore, the auxiliary chemotherapy after surgical treatments should be routinely performed to these patients. The accurate assessment of regional LNM after surgical treatments is critical for the selection of therapeutic plans for CRC patients and the selection of lymph node (LN) dissection in CRC surgeries (Sepulveda et al., 2017).

The <sup>18</sup>F-fluorodeoxyglucose (FDG) positron emission tomography (PET)/computed tomography (CT) imaging is a non-invasive examination method; it combines the morphology and the functional information, which is one of its advantages; it is important to the tumor diagnosis, differential diagnosis, clinical staging, curative effect monitoring, and the determination of radiotherapy plans (Xu and Jiang, 2017; Cavo et al., 2017; Chirindel et al., 2017). PET/CT can indicate more metastasis focuses of CRC through one-shot imaging, which provides important value for clinical

\* Corresponding author: Radiology department, Shengjing Hospital Affiliated to China Medical University, No. 36 Sanhao Street, Heping District, Shenyang 110000, China.

E-mail address: [radioliuzhaoyu@yeah.net](mailto:radioliuzhaoyu@yeah.net) (Z. Liu).

Peer review under responsibility of King Saud University.



Production and hosting by Elsevier

decision-making of CRC treatments. Innumerable researches have gradually recognized the values of PET/CT examination in the diagnosis, staging (preoperative staging and postoperative staging), and postoperative follow-ups of primary CRC.  $^{18}\text{F}$ -FDGPET/CT imaging is one of the important imaging extermination methods for preoperative staging of CRC (Zou et al., 2017);  $^{18}\text{F}$ -FDGPET/CT imaging can be used to evaluate the tumor infiltration (T staging) of CRC, the LNM of CRC (N staging), and the remote metastasis of the tumor (M staging), which can provide accurate clinical staging and preoperative evaluations (Lucia et al., 2018). In recent years, with the development of computer technologies, the development of medical imaging analysis methods has been greatly promoted. Automated methods such as artificial intelligence, neural networks, and deep learning have gradually been applied in medical imaging analysis. Texture analysis is a mathematical algorithm that describes the gray level intensity relationship or the positional relationship between pixels and voxels in images, it has the advantage of being able to describe the heterogeneity of gray level distribution in images (Solnes et al., 2017). Recently, the method of texture analysis has gradually been applied to the analysis of medical images.

Although medical imaging analysis based on computer technology has been unprecedentedly developed in recent years, the criteria for LNM of malignant tumors are still difficult to define, and the accuracy (Acc) and sensitivity (Sen) of PET/CT diagnosis in the area need to be improved. The errors caused by the above factors would affect the selection of the therapeutic plans (Wong et al., 2018). In multivariate analysis of relevant clinical information, PET image information, and grain factors of CRC patients can be performed and the diagnostic model of LNM in the region of CRC is constructed, the diagnosis or prediction Acc of LNM of CRC would be improved, and more accurate clinical staging of patients would be achieved. Therefore, the association among the LNM in the region of CRC and the relevant clinical information, PET/CT image data, and PET grain factors of CRC patients was investigated, the regional LNM diagnostic model was built, and the effects of the diagnostic model on diagnosing LNM in the region of CRC were evaluated.

## 2. Materials and methods

### 2.1. Research objects and data collection

From April 2017 to August 2019, 200 CRC patients underwent  $^{18}\text{F}$ -FDG PET/CT examination in the PET Center of Shengji Hospital Affiliated to China Medical University were retrospectively collected, in which the eligible cases were screened. The included patients were grouped as the regional LNM positive (+) group and the regional LNM negative (–) group. The case-related demographic data (gender and age), the locations of the CRC tumors, the existence or non-existence of ileus, and the sizes of the tumors were retrospectively collected. Relevant information such as pathological types, degrees of differentiation, tumor infiltration, existence or non-existence of mucus components, the sum of LNs being examined, the sum of metastatic LNs, positions of the metastatic LNs in the postoperative pathological reports of CRC patients were collected. In the research, LNM was defined in terms of patients.

### 2.2. Inclusion criteria and exclusion criteria

Inclusion criteria: newly diagnosed CRC patients who did not accept any anti-tumor treatments before PET/CT scans; patients who went through radical resection of CRC or tumor resection

within 2 weeks after PET/CT scans; the medical records must be complete.

Exclusion criteria: patients with more than one colorectal lesion; patients whose PET images showed a significant increase in colorectal metabolic diffusion; patients whose CRC lesion length was <2.0 cm; patients whose sum of LNs found in the postoperative pathological results was <12; patients whose radioactive concentrated imaging results of CRC lesions and those of the bladder urine had unclear boundaries; patients whose PET images were of poor quality and cannot be evaluated.

### 2.3. Imaging methods

The patients fasted for >6 h. In the calm states, they were injected with  $^{18}\text{F}$ -FDG 183–395 MBq intravenously through the T-pipes; then, the patients lied calmly in a dark room for about 1 h; after urination, patients received PET/CT imaging scans. Before injecting  $^{18}\text{F}$ -FDG, the plasma glucose levels of patients should be assayed through routine examinations; the plasma glucose levels of patients should be <7.0 mmol/L; for patients with diabetes, the plasma glucose levels should be controlled before the PET/CT scans. The imaging examination included CT scans and PET emission scans, with the scanning range, starting from the middle thigh to the calvarium. BiographmCTx acquisition parameters: the CT voltage was 120 kV, the current was automatic milliamperes, the pitch was 0.55, the single-turn rotation time of the tube was 1.0 s, and the slice thickness was 3 mm; the PET emission scans adopted three-dimensional acquisition, with the rate of 2 min/bed. PET reconstruction used the ordered subset expectation maximum (OSEM) iteration (OSEM), and image attenuation correction used CT scan data. After the CT scan was completed, the data was transmitted to the Siemens workstation, and the cross-section reconstruction was performed with a slice thickness of 2.0 mm.

### 2.4. ROI plotting of PET images and the extraction of PET grain factors

The PET sequences and CT sequences of the patients were opened in the nuclear medicine image analysis software to generate the fused images; under the guidance of the professional nuclear medicine physicians, the lesions of CRC were found; on the maximum intersecting surfaces of the tumors, the automatic plotting tool of the software was used to plot the regions of interest (ROI) of the tumors with SRO = 2.5; after the ROI was successfully plotted, the radioactive concentrated images of the CRC lesions from the transverse, sagittal, and coronal positions respectively to determine the existence or non-existence of all the ROI in the concentrated images and the existence or non-existence of radioactive concentrated images of non-CRC lesions in the ROI. If the plotted areas contained non-CRC lesions, the three-dimensional areas were further adjusted. A small amount of sigmoid colon cancer radioactive abnormal concentrated images was closely connected to uterus urine radioactive concentrated images; the automatic plotting cannot accurately plot the boundaries of CRC radioactive abnormal concentrated images; therefore, these cases were excluded. All the plotted ROI were confirmed by two experienced PET/CT diagnosticians. In the case of disagreement over the ranges of the ROI, the post-discussion opinion was taken as the final result. Finally, all the obtained ROI were saved in DICOM format and were exported.

The PET sequences and DICOM data of patients, and their corresponding ROI were imported into the image texture analysis toolbox to observe and confirm whether the PET images of the CRC patients were correctly matched with the corresponding ROI. The parameters were adjusted; after the gray level was discretized into 64 bits, each voxel in the ROI was re-collected; through various matrices and methods, the extracted texture characteristic param-

eters were 42 in total, including 4 first-level grain factors, 12 s-level grain factors, 22 advanced grain factors, and 4 grain factors extracted by texture characteristic coding matrix of the texture characteristic coding method (Wang and Evans, 2017; Strömvall et al., 2017). At the same time, the traditional PET image parameters including SUVmax and TLG were extracted. The first-level grain factors were obtained according to the statistics data of the SUV gray level histogram; the second-level grain factors were extracted by the gray level concurrence matrix (GLCM) and the neighboring gray level dependence matrix (NGLDM); the advanced grain factors were extracted by the gray level run-length matrix (GLRLM) and the gray level size zone matrix (GLSZM). The grain factors extracted by the grain characteristic coding matrices included roughness, homogeneity, average convergence, and variance (Feldens, 2017; Liu et al., 2018).

### 2.5. PET/CT image analysis

The observation range of PET/CT images was the LNs in the drainage areas of CRC, including the paracolic LNs, the intermediate LNs, and the mesenteric LNs. The  $^{18}\text{F}$ -FDG PET/CT images of CRC patients were analyzed by two experienced PET/CT diagnosticians. The diagnosticians observed the radioactive concentrations of LNs on the cross-sectional PET/CT fused images. The boundaries of the multiple LNs with a higher degree of radioactive concentrations obtained by visual observation were used to plot the ROI, the SUVmax value was measured separately, and the highest SUVmax value was finally recorded. Meantime, based on the  $^{18}\text{F}$ -FDG PET/CT complete imaging, the remote metastasis of patients was determined.

The sizes and distributions of LNs in the drainage areas of CRC were observed on CT images, and the short dimension of the largest LNs in the drainage area of CRC was measured. The existence or non-existence of the clustered LNs was observed and recorded. In the case of disagreement, the post-discussion opinion was taken as the final result. The clustered LNs were defined as three or more LNs distributed in groups. According to the measured LN SUVmax and LN short-dimension data, the SUVmax and short-dimension data of each patient's LNs were grouped according to SUVmax 22.5 and LN short-dimension  $\geq 1.0$  cm, respectively; the number of patients in each group was finally summarized.

### 2.6. Regional LNM diagnostic model construction based on clinical information and grain factors

The single-variable analysis summarized the statistical differences in the factors between the patients in the regional LNM+ and LNM- groups. In the grain factors, the factor with the variance of AUC being  $< 0.5$  was included as a factor that had no influences on the model into the regression model. The independent variables included 6 factors, i.e. the clinical data of remote metastasis and intestinal obstruction, the PET/CT image factors of regional LN SUVmax, regional LN short dimension, and 2 PET grain factors of roughness and average convergence extracted by grain characteristic coding method; based on the dependent variable, i.e. the post-operative pathological results of existence or non-existence of regional LNM, a regional LNM diagnostic model was established by logistic regression. In the model, the PET/CT image data and grain factors were continuous variables. First, these data and factors were converted into binary variables according to the cut-off points; then, they were included in the model. The difference of the regression model that was statistically significant was concluded. The 5 independent variables included in the model were intestinal obstruction, regional LN SUVmax, regional LN short dimension, and the grain factors of roughness and average convergence. The constructed mathematical model was:

$$P = \frac{1}{1 + e^{-Z}} \quad (1)$$

Z was the sum of the individual independent variables multiplied by their OR numbers.

### 2.7. Statistic analysis

The statistic analysis was conducted by using the IBM SPSS 20.0 statistical software. The receiver operator characteristic (ROC) curves were processed by Medcalc software. The measurement data in normal distribution or approximated to normal distribution were articulated in the form of  $\bar{x} \pm s$  (mean number  $\pm$  standard deviation). The statistical measures that were not in normal distribution were articulated in the form of median (interquartile range). The bilateral test was applied to each statistical test. If the P value was  $< 0.05$  ( $P < 0.05$ ), the difference was considered statistically significant.

Univariate analysis: the Chi-square ( $\chi^2$ ) test conducted differential analysis of count data of patients in the LNM+ group and the LNM- group. The comparative analysis of measurement data in normal distribution with equal variance was tested by two-sample *t*-test; the comparative analysis of measurement data that were not in normal distribution or the variance was unequal was tested by the Mann-Whitney *u* test. Comparisons between diagnostic Sen and specificity (Spe) of methods for LNM in different diagnostic areas were performed by using the paired  $\chi^2$  test (McNemar). The consistency among different diagnostic methods was compared by using the Kappa test.

Multivariate analysis: the existence or non-existence of regional LNM was taken as the independent variable; statistically significant data obtained from above univariate analysis were taken as dependent variables; the Wald test was used for stepwise regression, and the step probability was entering  $P \leq 0.05$ , delete  $P > 0.10$ . A diagnostic model of CRC regional LNM containing clinical information, PET image information, CT image information, and grain factors were established.

ROC curve analysis: After plotting the ROC curves, the area under the curve (AUC) was computed to assess the efficacy of each examination in diagnosing CRC regional LNM. The larger the AUC was, the higher the diagnostic efficiency of the diagnostic method was. The cut-off points of CRC regional LNM predicted by each factor were calculated through the Youden Index ( $YI = \text{Sen} + \text{Spe} - 1$ ), and the Sen and Spe at the cut-off points were obtained.

## 3. Results and discussion

### 3.1. Analysis of basic information of the CRC patients

Retrospectively, 200 medical cases of CRC patients were included in the research based on the inclusion and exclusion criteria. All included patients underwent surgeries within two weeks after PET/CT scans. The CRC patients in the regional LNM+ group were 92 cases in total (accounted for 46%), with the average age of  $61.5 \pm 11.6$  years and the range of age was 31–79 years. The CRC patients in the regional LNM- group were 108 cases in total (accounted for 54%), with the average age of  $63.4 \pm 10.3$  years old and an age range of 40–81 years old. Based on the collected clinical data, the included CRC patients were submitted to TNM staging, including 10 cases (5%) in stage 1, 92 cases (46%) in stage 2, 68 cases (34%) in stage 3, and 30 cases (30%) in stage 4 (15%).

The univariate analysis showed no statistically significant differences in ages, genders, tumor positions, the maximum tumor dimension, the existence or non-existence of mucus components, the differentiation of tumors, and the relevant tumor

markers CEA, CA199, CA724, and TLG ( $P > 0.05$  without exceptions), as shown in Fig. 1. The research results showed statistically significant differences in TNM staging, intestinal obstructions, tumor infiltration, regional LN SUVmax, regional LN minimum dimension, and the existence or non-existence of remote metastasis between the CRC patients in the positive group and the negative group ( $P < 0.05$  without exceptions), as shown in Fig. 2.

### 3.2. Efficacy and comparisons of CRC regional LN minimum width and regional LN SUVmax on the diagnosis of LNM

Among all the CRC patients researched in this study, 92 patients were with positive regional LNM, the maximum LN short dimension was  $1.13 \pm 0.39$  cm; in addition, 108 patients were with negative regional LNM, the maximum LN short dimension was  $0.64 \pm 0.26$  cm; the regional LN short dimensions between patients in + and – groups were found to be statistically significant ( $P < 0.05$ ). The regional LN SUVmax of regional LNM+ patients was 3.7 (2.1, 6.9), and the regional LN SUVmax of regional LNM- patients was 1.5 (0.6, 2.5). The differences in regional LN SUVmax between patients in both groups had statistical significance ( $P < 0.05$ ). Through ROC curve analysis, the regional LN short dimension prediction AUC of LNM was 0.742, the 95%CI was 0.667–0.811; if the regional LN short dimension value was

1.19 cm, the Youden index reached a maximum of 0.388, at the moment, the Sen of predicting regional LNs metastasis was 42.4%, and the Spe was 97.1%. The AUC of regional LN SUVmax predicted LNM was 0.753, and the 95%CI was 0.681–0.823; if the cut-off points of regional LN SUVmax was 3.27, the Youden index reached a maximum of 0.408, at the moment, the Sen of predicting regional LNs metastasis was 55.6%, and the Spe was 85.8% (see Fig. 3).

### 3.3. The efficacy of clustered LNs in the adjacent and draining areas of CRC in diagnosing regional LNM

Of all the patients, 122 cases (61.0%) had clustered LNs in the adjacent and draining areas of CRC, of which 62 cases were CRC regional LNM+ patients and 60 cases were regional LNM- patients. In addition, 79 (39.5%) cases had no clustered LNs in the adjacent and draining areas of CRC, including 31 cases of regional LNM+ CRC and 48 cases of LNM-. LNM+ patients and LNM- patients were not significant in statistics ( $P > 0.05$ ). The typical cases were shown in Fig. 4.

### 3.4. Diagnostic efficacy of regional LNM diagnostic model

Through the analysis of ROC curves, the AUC of the diagnostic model in diagnosing regional LNM of CRC patients was 0.861

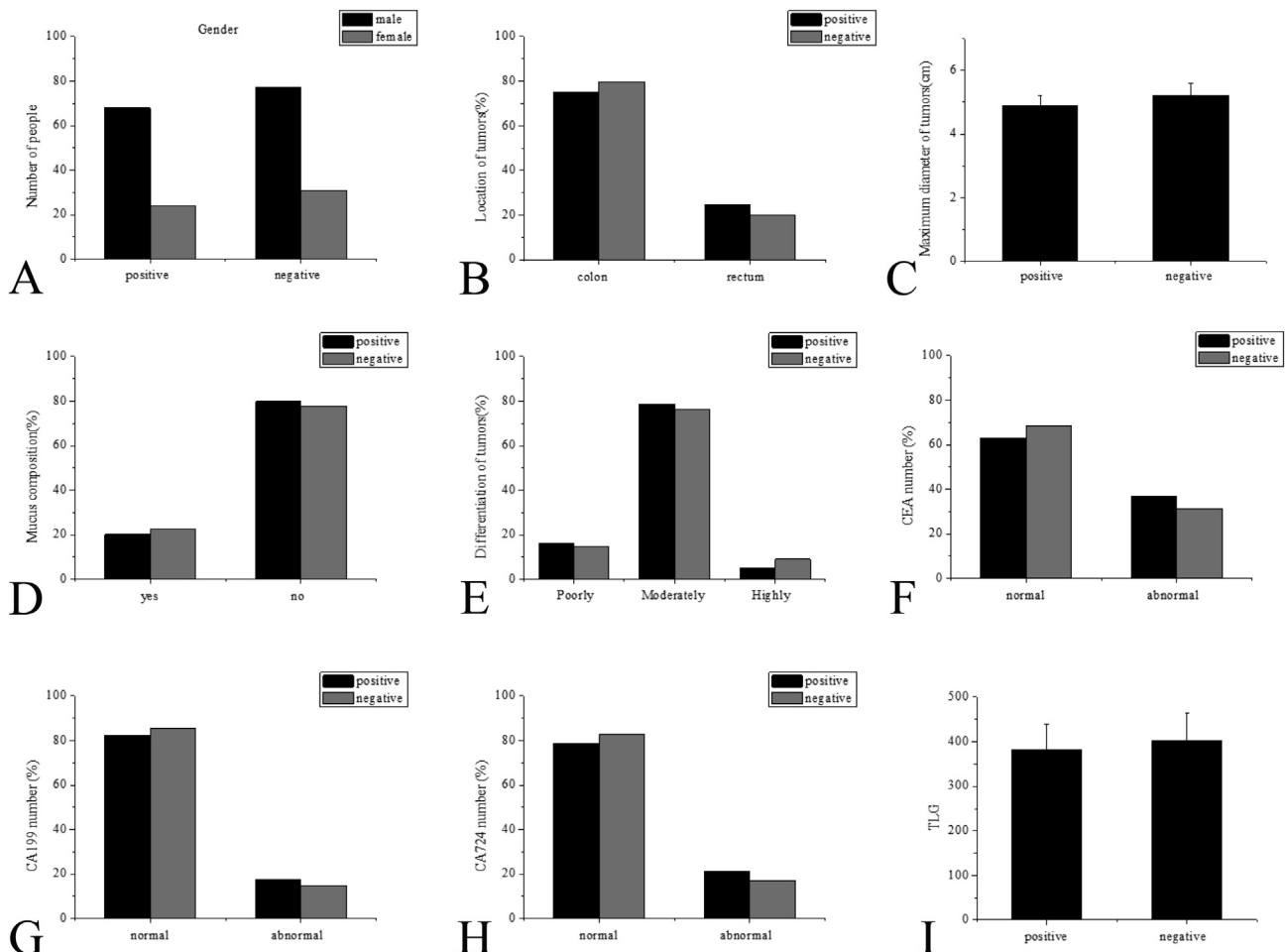


**Fig. 1.** Factor analysis (no statistical differences) ( $P > 0.05$ ) A: Gender comparison; B: Tumor location comparison; C: Comparison of the maximum tumor dimension; D: Comparison of mucus components; E: Tumor grade comparison; F: Comparison of relevant tumor marker CEA; G: Comparison of relevant tumor marker CA199; H: Comparison of relevant tumor marker CA724; I: Comparison of relevant tumor marker TLG.

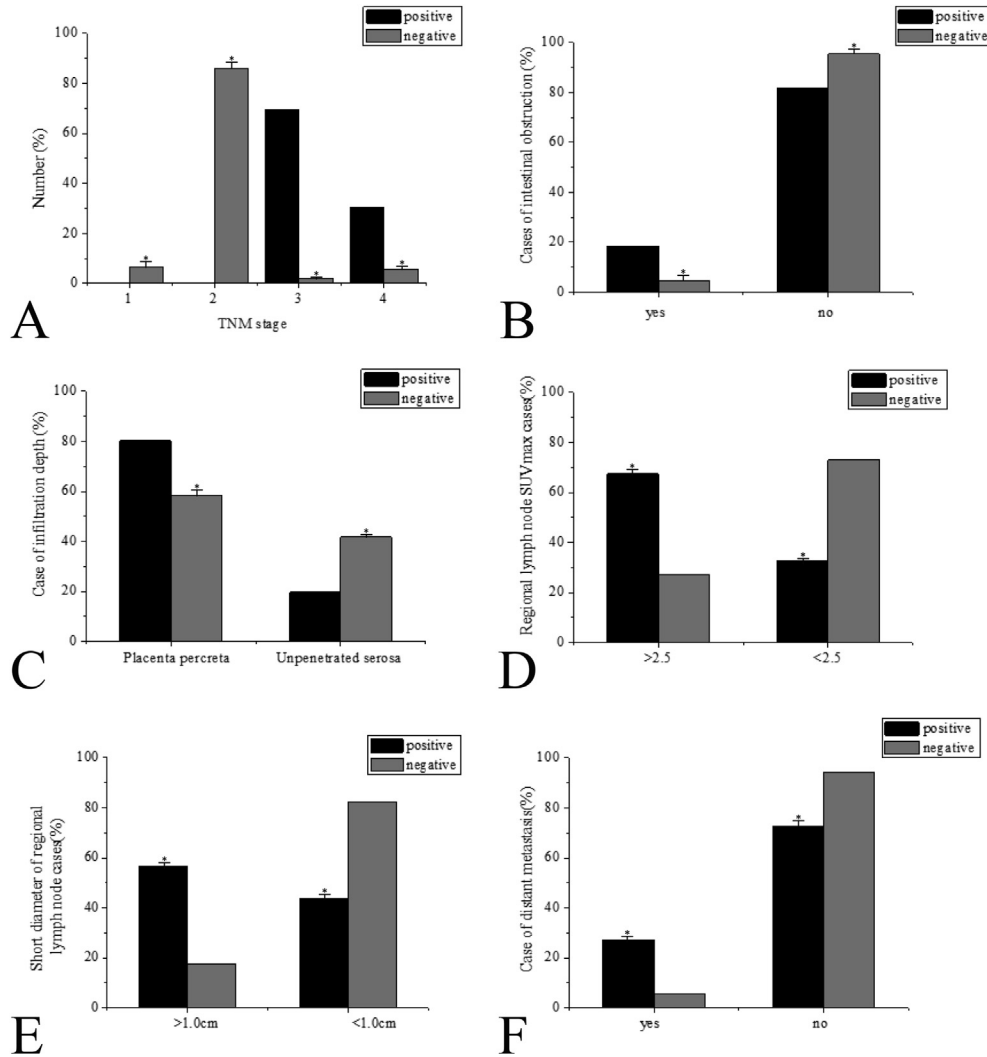


**Fig. 2.** Factor analysis (The two groups had significant differences, \*P < 0.05) A: Comparison of CRC TNM staging; B: Intestinal obstruction comparison; C: Comparison of tumor infiltration; D: Comparison of regional LN SUVmax; E: Comparison of regional LN minimum width; F: Comparison of remote metastasis of CEA.

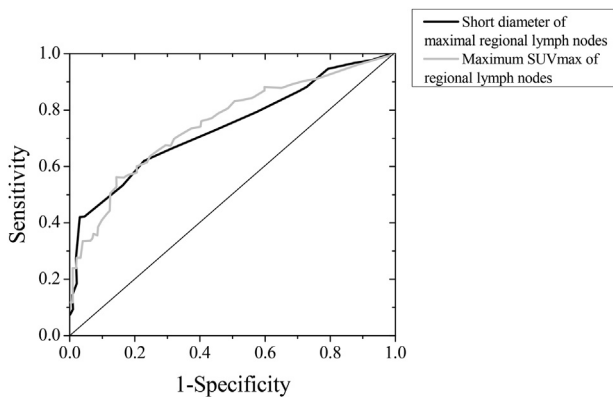


**Fig. 3.** Regional LN short dimension and regional LN SUVmax predicted ROC curve of CRC regional LNM.

(the 95%CI was 0.811–0.907,  $P < 0.001$ ); if the prediction probability value was 0.342, the Youden index reached a maximum of 0.545. At the moment, the Sen, Spe, and Acc of the diagnosis of regional LNs metastasis performed by the diagnostic model were 77.8%, 75.9%, and 77.4% respectively.

### 3.5. Comparison of the efficacy and consistency of the diagnostic model of LNM in CRC with other diagnostic criteria

As shown in Fig. 5, through the analysis of ROC curves, compared with the PET diagnostic criteria, CT diagnostic criteria, and PET/CT diagnostic criteria, the diagnostic efficacy of the diagnostic model was significantly better than other diagnostic methods; based on the Youden Index Method, if the P value was 0.338, the Sen of the diagnostic model was considerably greater than that of the CT diagnosing criteria and the PET/CT diagnostic criteria; however, the differences in Sen between the diagnostic model and the PET/CT diagnostic criteria were significant in statistics ( $P > 0.05$ ). Besides, the diagnostic Spe between the diagnostic model and other diagnostic methods were found to have no statistical significance (see Fig. 6).

## 4. Discussion

CRC is a widespread malignant tumor in the gastrointestinal tract. The disease can be spread to other tissues and organs through lymphatic and blood circulation, as well as direct extension. The diagnosis can be made according to clinical manifesta-

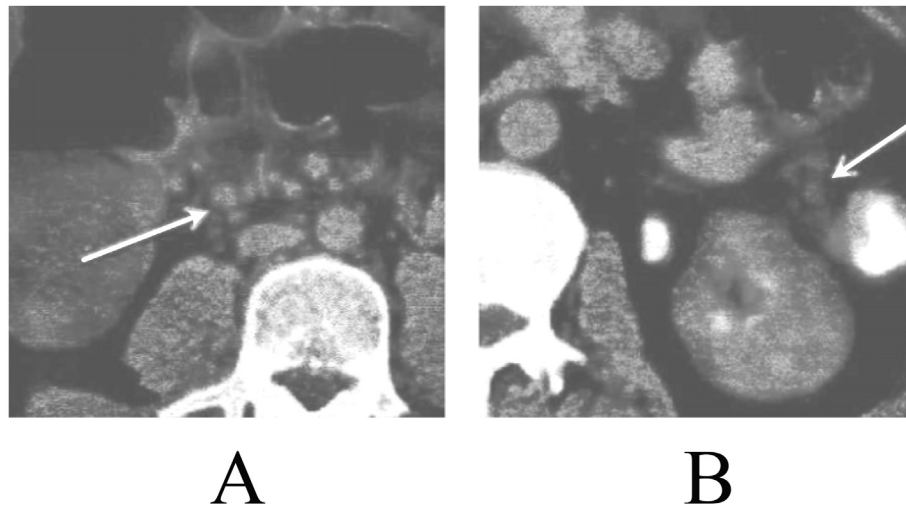


**Fig. 4.** The fused PET/CT images, with arrows indicating the clustered LNs A: PET/CT fused images of CRC regional LNM+ patients B: PET/CT fused images of regional LNM- patients.

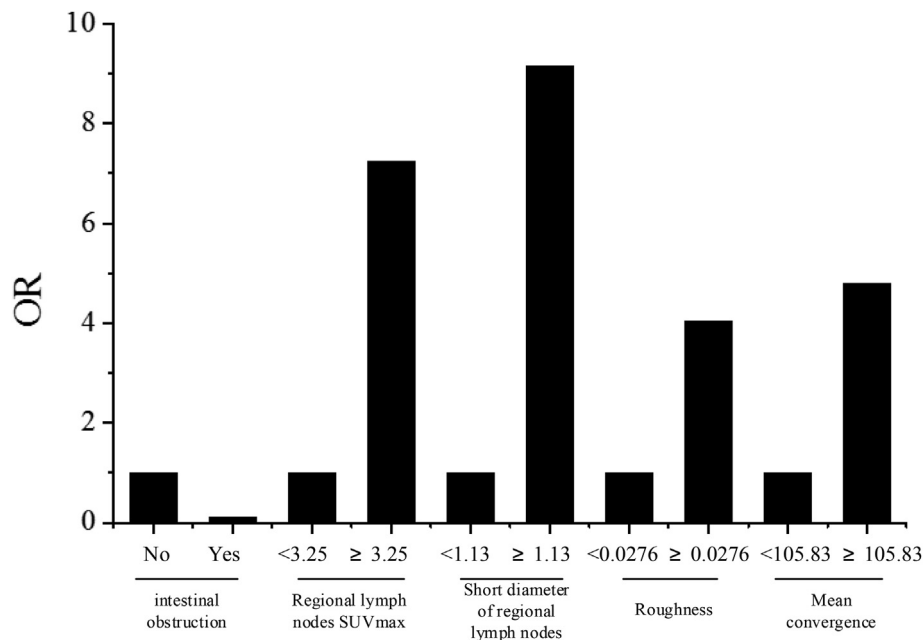


**Fig. 5.** Risk factors of LNM in CRC (Logistic regression).

tions, X-ray barium enema results, or fiberoptic colonoscopy. The  $^{18}\text{F}$ -FDG PET/CT imaging is a non-invasive examination method for tumors, which is vital for tumor diagnosis, clinical staging, efficacy monitoring, and the development of radiotherapy plans of tumors. However, in diagnosing the LNM of malignant tumor, there are certain limitations in medical imaging technology. Therefore, this study analyzed the relationship between clinical information, PET/CT image data, and PET grain factors of CRC and LNM of CRC and established a regional LNM diagnosis model to explore the application effect of the model on the diagnosis of CRC LNM.

Through the analysis of data of CRC patients, it was found that the most preferable metastasis route was regional LNM. The  $^{18}\text{F}$ -FDG PET/CT scans were applied to examine the malignant tumors of patients; combined with the grain factors, the diagnostic model was constructed. The basic information of patients was analyzed initially. The CRC patients in the regional LNM+ group were 92 cases in total (accounted for 46%), with the average age of

$61.5 \pm 11.6$  years and the range of age was 31–79 years. The CRC patients in the regional LNM- group were 108 cases in total (accounted for 54%), with the average age of  $63.4 \pm 10.3$  years old and an age range of 40–81 years old. The research results showed no statistically significant differences in ages, genders, tumor positions, the maximum tumor dimension, the existence or non-existence of mucus components, the differentiation of tumors, and the relevant tumor markers CEA, CA199, CA724, and TLG ( $P > 0.05$  without exceptions). The research results showed statistically significant differences in TNM staging, intestinal obstructions, tumor infiltration, regional LN SUVmax, regional LN minimum dimension, and the existence or non-existence of remote metastasis between the CRC patients in the LNM+ group and the LNM- group ( $P < 0.05$  without exceptions). Through the comparisons between the diagnostic model proposed in the research and other diagnostic methods, it was found that the diagnostic efficacy of the proposed diagnostic model was obviously higher than other

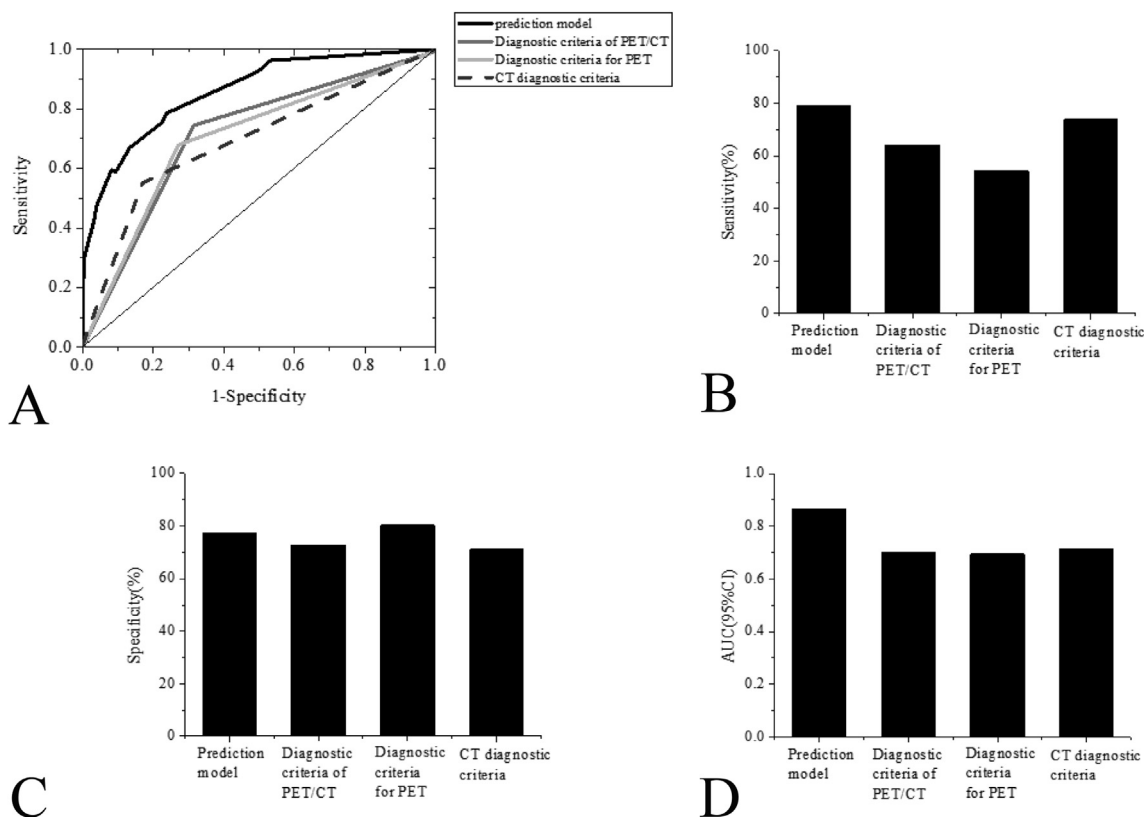


**Fig. 6.** Comparison of the proposed diagnostic model with other diagnostic criteria A: The ROC curves of the diagnosis model and other diagnostic criteria in diagnosing CRC regional LNM; B: Comparison in Sen between the diagnostic model and other diagnostic criteria; C: Comparison in Spe between the diagnostic model and other diagnostic criteria; D: Comparison in AUC between the diagnostic model and other diagnostic criteria.

methods. Therefore, it was concluded that the diagnostic model was of significant values in clinical applications.

### Acknowledgement

This study was funded by a grant from the National Natural Science Foundation of China (Project No. 81871465).

### References

- Arnold, M., Sierra, M.S., Laversanne, M., et al., 2017. Global patterns and trends in colorectal cancer incidence and mortality. *Gut* 66 (4), 683–691.
- Cavo, M., Terpos, E., Nanni, C., et al., 2017. Role of 18F-FDG PET/CT in the diagnosis and management of multiple myeloma and other plasma cell disorders: a consensus statement by the International Myeloma Working Group. *Lancet Oncol.* 18 (4), e206.
- Chirindel, A., Chaudhry, M., Blakeley, J.O., et al., 2017. 18F-FDG PET/CT qualitative and quantitative evaluation in neurofibromatosis type 1 patients for detection of malignant transformation: comparison of early to delayed imaging with and without liver activity normalization. *Nagoya J. Med. Sci.* 79 (1), 9–16.
- Feldens, P., 2017. Sensitivity of grain parameters to acoustic incidence angle in multibeam backscatter. *IEEE Geosci. Rem. Sens. Lett.* PP (99), 1–5.
- Flemer, B., Lynch, D.B., Brown, J.M.R., et al., 2017. Original article: Tumour-associated and non-tumour-associated microbiota in colorectal cancer. *Gut* 66 (4), 633–643.
- Liu, Y., Deng, J., Wei, W., et al., 2018. Effect of grain parameters on cutting performance of flank-faced grain carbide tools in dry cutting of green Al<sub>2</sub>O<sub>3</sub> ceramics. *Ceramics Int.* 44 (11), S0272884218310198.
- Long, A.G., Lundsmith, E.T., Hamilton, K.E., 2017. Inflammation and colorectal cancer. *Curr. Colorectal Cancer Rep.* 13 (4), 341–351.
- Lucia, F., Visvikis, D., Desserot, M.C., et al., 2018. Prediction of outcome using pretreatment 18F-FDG PET/CT and MRI radiomics in locally advanced cervical cancer treated with chemoradiotherapy. *Eur. J. Nucl. Med. Mol. Imag.* 45 (5), 768–786.
- Muro, K., 2017. Systemic chemotherapy for metastatic colorectal cancer – Japanese Society for Cancer of the Colon and Rectum (JSCCR) Guidelines 2016 for treatment of colorectal cancer. *Nihon Shokakibyō Gakkai Zasshi* 114 (7), 1217–1223.
- Rex, D.K., Boland, C.R., Dominitz, J.A., et al., 2017. Colorectal cancer screening: recommendations for physicians and patients from the U.S. Multi-Society Task Force on Colorectal Cancer. *Gastroenterology* 112 (7), S0016508517355993.
- Sepulveda, A.R., Hamilton, S.R., Allegra, C.J., et al., 2017. Molecular biomarkers for the evaluation of colorectal cancer. *J. Mol. Diagn.* 19 (2), 187–225.
- Solnes, L.B., Jones, K.M., Rowe, S.P., et al., 2017. Diagnostic value of 18F-FDG PET/CT versus MRI in the setting of antibody-specific autoimmune encephalitis. *J. Nucl. Med.* 58 (8), 1307–1313.
- Strömvall, K., Thysell, E., Halin, B.S., et al., 2017. Aggressive rat prostate tumors reprogram the benign parts of the prostate and regional lymph nodes prior to metastasis. *PLoS One* 12 (5), e0176679.
- Wang, T.S., Evans, D.B., 2017. Commentary on: occult lymph node metastasis and risk of regional recurrence in papillary thyroid cancer after bilateral prophylactic central neck dissection: a multi-institutional study. *Surgery* 161 (2), 472–474.
- Wong, S.L., Faries, M.B., Kennedy, E.B., et al., 2018. Sentinel lymph node biopsy and management of regional lymph nodes in melanoma: american society of clinical oncology and society of surgical oncology clinical practice guideline update. *J. Clin. Oncol.* 36 (4), 399.
- Xu, K., Jiang, B., 2017. Analysis of mucosa-associated microbiota in colorectal cancer. *Med. Sci. Monit. Int. Med. J. Exp. Clin. Res.* 23, 4422–4430.
- Yu, J., Feng, Q., Wong, S.H., et al., 2017. Metagenomic analysis of faecal microbiome as a tool towards targeted non-invasive biomarkers for colorectal cancer. *Gut* 66 (1), 70–78.
- Zou, Y., Tong, J., Leng, H., et al., 2017. Diagnostic value of using 18F-FDG PET and PET/CT in immunocompetent patients with primary central nervous system lymphoma: a systematic review and meta-analysis. *Oncotarget* 8 (25), 41518–41528.